MICHIGAN STATE
UNIVERSITY

National Superconducting Cyclotron Laboratory

PRODUCTION OF A = 6,7 NUCLIDES IN THE $\alpha + \alpha$ REACTION AND COSMIC RAY NUCLEOSYNTHESIS

DAVID J. MERCER, SAM M. AUSTIN, J.A. BROWN,
S.A. DANCZYK, S.E. HIRZEBRUCH, J.H. KELLEY,
T. SUOMIJÄRVI, D.A. ROBERTS, T.P. WALKER

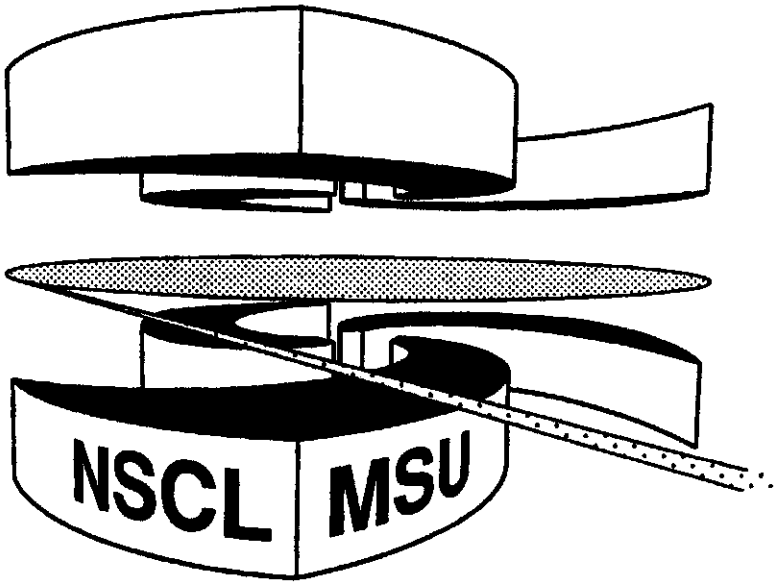

MSUCL-1176

OCTOBER 2000

Submitted to Physical Review C

Production of $A = 6, 7$ Nuclides in the a + α Reaction and Cosmic Ray Nucleosynthesis

David J. Mercer[1,2*], Sam M. Austin[2,3†], J. A. Brown[2‡], S. A. Danczyk[2,3], S. E. Hirzebruch[2], J. H. Kelley[2,3§], T. Suomijärvi[2,4] D. A. Roberts[5], T. P. Walker[6]

[1]Nuclear Physics Laboratory, University of Colorado, Boulder, CO 80309-0446

[2]National Superconducting Cyclotron Laboratory, Michigan State University, East Lansing, MI 48824

[3]Department of Physics and Astronomy, Michigan State University, East Lansing, MI 48824

[4]Institute de Physique Nucléaire, IN_2P_3-CNRS, 91406 Orsay, fiance

[5]Department of Physics, University of Michigan, Ann Arbor, MI, 48109

[6]Department of Physics, The Ohio State University, Columbus OH 43210

(September 18, 2000)

*Present Address: NIS-5 Group, LANL, Los Alamos NM 87545; Electronic address: mercer@lanl.gov

†Electronic address: austin@nscl.msu.edu

‡Present address: Physics Department, Millikin University, Decatur IL 62522

§Present address: Department of Physics, North Carolina State University, Raleigh NC 27695

Abstract

Cross sections for production of ^{6}He, ^{6}Li, ^{7}Li, and ^{7}Be in the $\alpha + \alpha$ reaction were measured at bombarding energies of 159.3, 279.6, and 619.8 MeV, and are found to decrease rapidly with increasing energy. These cross sections are essential for the calculation of the rate of nucleosynthesis of the lithium isotopes in the cosmic rays and thereby play a key role in our understanding of the synthesis of Li, Be, and B. The results for ^{6}Li differ significantly from the tabulated values commonly used in cosmic-ray production calculations and lead to lower production of ^{6}Li.

Typeset using REVTEX

I. INTRODUCTION

The origins of the light elements Li, Be, and B (LiBeB) differ from that of the other nuclides. Most elements are formed in stars, but LiBeB are rapidly consumed by radiative capture reactions in stellar centers and must therefore be synthesized in cooler or more tenuous environments. It had been generally accepted [1–4] that ^{6}Li, ^{9}Be, ^{10}B, and some ^{11}B were made in the galactic cosmic rays (GCR) by the interaction of fast GCR protons and α particles with interstellar targets of carbon, nitrogen, oxygen (CNO) or He (and vice-versa); ^{2}H, ^{3,4}He, and the primeval abundance of ^{7}Li were made in the Big Bang.

Recent measurements of abundances in metal-poor stars formed early in the life of the galaxy challenge the details of the GCR picture. The abundance of ^{9}Be rises linearly with the iron abundance [5,6]. It has been argued (see [7,8] and references therein) that this means that heavy cosmic rays (CNO) incident on interstellar hydrogen and helium are responsible for the synthesis of LiBeB. Others [9] argue that the original process remains viable. In any case the $\alpha + \alpha$ reaction plays a major role in production of ^{6,7}Li, particularly if light cosmic rays are responsible for their synthesis [6], since the interstellar medium contains little CNO in the early galaxy. Recent models [8,10] show that ^{6}Li is marginally produced in the observed quantity, so that accurate estimates of the Li-producing reactions are required for a rigorous test of these models.

Unfortunately, the $\alpha + \alpha$ cross sections [11] are not known at high enough energies for such purposes—no data are available for ^{6}Li production above 200 MeV, although the cosmic ray α-particle flux remains strong beyond this energy [4]. The predicted early-galaxy abundances of ^{6}Li can vary significantly (for example, by a factor of two in the model of Ref. [12]), depending on how the lower energy cross sections are extrapolated to higher energy.

To provide the necessary data, we measured angular distributions of $A = 6, 7$ ejectiles from the $\alpha + \alpha$ reaction for alpha energies between 159 and 620 MeV, and integrated these distributions to obtain the total production cross sections for masses 6 and 7. We find that the cross sections fall rapidly, essentially exponentially, with increasing bombarding

energy, becoming small enough that $\alpha + \alpha$ will not contribute significantly to cosmic ray nucleosynthesis at energies above the measured range (to 620 MeV).

II. EXPERIMENTAL METHODS

The cross sections at bombarding energies above 160 MeV were expected to be small, leading to potentially severe problems of background scattering and long collection times if a traditional gas cell approach was used, as in previous measurements [13–16]. To avoid these problems, we employed two novel techniques: (1) the detectors were placed inside the target gas volume to eliminate background scattering from target cell walls and windows, and (2) a telescope system with a wide and continuous acceptance in laboratory scattering angle was used to reduce data collection time. Details of the target, detector telescopes, beam, and angle and acceptance calibrations are given below.

The target was natural helium gas, >99.99% pure, which filled the NSCL 92-inch scattering chamber; the gas pressure ranged from 370 to 408 torr (measured to $\pm 0.5\%$) and the temperature was 23°C. A schematic of the chamber is shown in Fig. 1. The chamber housed a remotely operable turntable on which the detectors were mounted, and the effective target was a cylinder of gas extending approximately 135 cm upstream and 15 cm downstream from the center of the turntable. The entrance window was a 6.4 μm Havar foil which was located 150 cm upstream from the turntable center and was partially blocked from view of the detectors by lead shielding. The chamber was evacuated on several occasions to check background from the entrance foil. Only at the most forward laboratory scattering angles ($\leq 7°$) were background subtractions for window scattering necessary, and these subtractions were smaller than 20% of the total observed yield at any angle.

A target ladder was located at the center of the turntable, and held secondary targets used for beam monitoring and calibration: a 47 mg/cm^2 carbon foil, a 0.5 mm diameter "pinhole," a 1 mm diameter vertical steel "needle," a 2 mm thick aluminum target with a 20 mm diameter hole, and a scintillator. This ladder was lowered completely out of the beam

path during data collection with the primary (helium) target.

Beams of α particles were provided by the NSCL K1200 Cyclotron at nominal energies of 160, 280, and 620 MeV. The lowest energy was chosen to allow direct comparison with results of [14], and the higher energies were chosen to span the region of astrophysical interest. All beams were fully stripped upon arrival at the scattering chamber. Up to 1.2 MeV is deposited in the entrance foil and target gas prior to the reaction, depending on the initial energy and point of scatter. The average bombarding energies, accounting for these losses and the 0.2 MeV uncertainty in the measured energy, were 159.3 ± 0.5 MeV, 279.6 ± 0.4 MeV, and 619.8 ± 0.3 MeV. The beam spot was checked by periodic insertion of two scintillators viewed by TV cameras, located at the turntable center and 170 cm upstream of turntable center. The beam radius at the turntable was ≤ 2 mm and the calculated half-angle divergence $\leq 0.5°$. Possible beam halo was monitored by periodically inserting the aluminum "hole" target and looking for scattered particles; no significant halo was observed. The unscattered beam was collected in a vacuum-isolated Faraday cup 2 meters downstream from the scattering chamber, and integrated beam current was found with $\pm 5\%$ uncertainty using a BIC Model 1000 current integrator.

Two detector telescopes were fixed to the turntable at beam height, one on each side of the beam. Each telescope consisted of a stack of two 1 cm tall $\times$ 9 cm wide charge-division position-sensitive silicon detectors (PSDs) and one 3 cm thick CsI(Tl) scintillator viewed by photodiodes, as shown in Fig. 2. In telescope 1 the PSDs had thicknesses of 320 μm (front) and 1000 μm (back), and were located 300 and 367 mm from the turntable center. In telescope 2, the PSDs had thicknesses of 300 μm (front) and 480 μm (back), and were located 300 and 363 mm from the turntable center, 80° clockwise from telescope 1. Standard electronics were used for signal amplification and data acquisition.

With the turntable centered, each telescope viewed a laboratory scattering angle range of 7°–60° simultaneously. Five different turntable settings were used during data collection; at a given scattering angle this provided independent measurements with a variety of solid-angle acceptance conditions. The turntable settings were centered (as shown in Fig. 1),

rotated $\pm 10°$ from the centered position, and rotated $\pm 20°$. The smallest laboratory angle observed was 4°, seen only by the telescope rotated closest to the beam for $\pm 20°$ settings.

The telescopes provided distinct particle identification for $A \leq 7$ ejectiles from characteristic ΔE-E signatures in the PSDs. In some kinematic situations the ejectile penetrated both PSDs and stopped in the CsI(Tl) scintillator; in this case the energy deposited in the scintillator was also used to aid particle identification. The mass resolution was about 0.4 amu FWHM, sufficient to distinguish ^{6}Li and ^{7}Li. The energy resolution was sufficient to distinguish elastically scattered ^{4}He from ^{4}He produced in inelastic channels such as $^4\mathrm{He}(\alpha, tp)^4\mathrm{He}$ ($Q = -19.8$ MeV); however, discrimination between the $^4\mathrm{He}(\alpha, d)^6\mathrm{Li}$ channel ($Q = -22.4$ MeV) and the $^4\mathrm{He}(\alpha, pn)^6\mathrm{Li}$ channel ($Q = -24.6$ MeV) was unreliable, particularly at the higher energies. It was not possible to distinguish the particle-stable first excited state in ^{7}Li or ^{7}Be (0.48 MeV and 0.43 MeV, respectively) from the ground state. The first excited state in ^{6}Li (2.18 MeV) decays immediately to $\alpha + d$ and does not contribute significantly to ^{6}Li production. The second excited state in ^{6}Li (3.56 MeV) is particle-stable, but it was not possible to distinguish it from the ground state. Since the primary concern of the present experiment is total production cross sections, these resolution limitations are not important.

For a valid event, both PSDs in a telescope must detect the scattered particle. The impact position on each PSD is inferred using standard charge-division techniques; from these impact positions and the known spacing between the PSDs it is possible to derive the scattering angle θ_{lab} and the scattering position z along the beam axis. The scattering angle is needed for computing the differential cross sections $d\sigma/d\Omega_{\mathrm{lab}}$, and the z position is needed to exclude particles that may have scattered in the Havar entrance foil. Angle calibration is performed by stepping each telescope through a pinhole-collimated α beam. The calibration was tested by reconstructing the tracks of particles scattered from a "needle" target protruding into the beam and from four 50μm Kapton foils that could be inserted at various locations along the beam path. Angular resolution was about 1.2° FWHM and was not degraded significantly when the chamber was filled with helium.

Differential cross sections are found from the observed yields according to

$$\frac{d\sigma(\theta)}{d\Omega_{\rm lab}} = \frac{Y(\theta)}{N_{\rm beam}\, f_{\rm live}\, \rho\, A(\theta)}, \tag{1}$$

where $Y(\theta)$ is the observed number of ejectiles at the laboratory scattering angle, here denoted by θ. $N_{\rm beam}$ is the number of incident particles, $f_{\rm live}$ is the detection system live fraction ($\approx 85\%$), and ρ is the target density (nuclei/cm^3). $A(\theta)$ is the detector acceptance (units of cm), equal to $\Delta\Omega x \epsilon T$ where $\Delta\Omega(\theta)$ is the effective solid angle, $x(\theta)$ is the effective length of the target region, ϵ is the detector efficiency, and T is the transmission fraction of scattered particles; it was greater than 99% and was taken to be unity.

Detector acceptance is a complicated function of scattering angle, turntable rotation, and details of mechanical alignment, and was determined by comparing our observed yields of elastically scattered ^{4}He at 160 MeV with the elastic differential cross section of Nadasen *et al.* [17] at a similar energy: equation (1) is solved for $A(\theta)$, and the resulting values are used to normalize the cross sections for all ejectiles at all three energies. This gives an estimated systematic error of 8% in $A(\theta)$ for typical laboratory scattering angles $\leq 40°$. A rough check on the acceptance was obtained using a simplified Monte Carlo simulation of the apparatus that omitted several known effects that were difficult to simulate. The Monte Carlo results agree with the empirically determined values of $A(\theta)$, typically within 12%, providing a level of assurance that the normalization procedure was reliable.

III. ANALYSIS AND RESULTS

The differential and total cross sections were measured for the four reactions ^{4}He$(\alpha, pp)^6$He, ^{4}He$(\alpha, \{d, pn\})^6$Li, ^{4}He$(\alpha, p)^7$Li, and ^{4}He$(\alpha, n)^7$Be. Because the target and projectile are identical, reaction products are distributed symmetrically about 90° c.m.; it is then sufficient to determine yields only for $\theta_{\rm c.m.} \leq 90°$. Detector acceptance for events from the backward c.m. hemisphere was rather low because the low energy ejectiles stopped in the 300 μm or 320 μm PSDs.

In all four reactions of interest, the kinematics are "folded" so that each laboratory angle corresponds to two c.m. scattering angles. For the two-body final states leading to ^{7}Li and ^{7}Be, it is a simple matter to distinguish between the two c.m. angles, because a larger ejectile energy is always associated with the more forward angle. There is an added complication for ^{6}Li and ^{6}He due to the three-body exit channels ^{6}He+$p+p$ and ^{6}Li+$p+n$. We determined a locus of ejectile energies corresponding to 90° c.m., as a function of laboratory scattering angle, from the kinematics result

$$p_{6\mathrm{Li}} \cos(\theta) = \gamma m_{6\mathrm{Li}} V_{\mathrm{c.m.}}, \tag{2}$$

where $p_{6\mathrm{Li}}$ is the momentum of ^{6}Li and $V_{\mathrm{c.m.}}$ is the velocity of the center of mass; all quantities are measured in the lab. The result is shown in Fig. 3. All ^{6}Li ejectiles observed with energies above this locus were attributed to the forward c.m. hemisphere, and those with less energy were attributed to the backward hemisphere. A similar procedure was used for the ^{6}He data. One can, in principle, distinguish the ^{4}He$(\alpha, d)^6$Li reaction from the ^{4}He$(\alpha, \{pn\})^6$Li reaction, as it is restricted to a band labeled "0 MeV" in Fig. 3. This was done in Refs. [14,16], but our energy resolution made it impossible; this is not a limitation for use of these cross sections in calculations of cosmic ray nucleosynthesis .

A. Differential cross sections

The differential cross sections (forward c.m. hemisphere only) for ^{6}Li and ^{6}He are shown in Fig. 4. The cross sections for ^{6}Li are forward peaked at all three energies. The cross sections for ^{6}He are also forward peaked and are roughly 1/8 as large as those for ^{6}Li. It was not possible to measure the cross section for ^{6}He at 620 MeV due to background contamination from ^{3,4}He ejectiles. We established that the ^{6}He cross section at 620 MeV is less than 25% of the cross section for ^{6}Li at this energy.

The differential cross sections (forward c.m. hemisphere only) for ^{7}Be and ^{7}Li are shown in Fig. 5. At 160 MeV the cross sections for both isotopes are forward-peaked with a

minimum at 90° c.m.; they are in excellent agreement with the measurements of Ref. [14] at a similar energy. The cross sections at 280 MeV are two orders of magnitude smaller, approaching the limit of our experimental method, and the minima at 90° disappear. At 620 MeV the cross sections were very small: fewer than two dozen possible ^{7}Li and ^{7}Be events were observed, roughly consistent with background. An upper limit is obtained at 620 MeV.

B. Total cross sections

Total cross sections for $A = 6$ production were found by extrapolating the differential cross sections to zero degrees, integrating over all laboratory angles corresponding to $\theta_{c.m.} \leq 90°$, and doubling to account for the $90° - 180°$ c.m. yield. The extrapolation to zero degrees is based on a linear fit through the three smallest-angle points ($\theta_{\rm lab} = 4.5, 6.5$, and $8.5°$). The extrapolated cross section $0 - 4.5°$ typically accounts for $10 - 20\%$ of the total cross section, and up to one third of the random uncertainty.

Total cross sections for $A = 6$ production are shown in Fig. 6 and Table I. For comparison, the cross sections from previous measurements in the 60-200 MeV range are also included. Errors given for the present experiment include the statistical, extrapolation, and normalization (8%) uncertainties, all added in quadrature.

The measured cross sections for ^{6}He and ^{6}Li differ from the values of Glagola *et al.* [14] near 160 MeV by about a factor of two. However, the present results agree with the reanalysis of the Glagola, *et al.* data by Mercer, Austin, and Glagola [18]. For both nuclides the total cross sections decrease rapidly with increasing energy. The solid lines in Fig. 6 are weighted exponential fits through all points shown, and have the functional forms (with the bombarding energy, E_α, in MeV and the slope for ^{6}He taken to be identical to that obtained for ^{6}Li)

$$\sigma_{\rm 6Li} = 66 \exp\left(-0.0159 E_\alpha\right) \text{ mb}, \tag{3}$$

$$\sigma_{\rm 6He} = 9.3 \exp\left(-0.0159 E_\alpha\right) \text{ mb}, \tag{4}$$

The exponential falloff is shallower than that suggested by Woo *et al.* [16], who report fits proportional to $\exp(-0.025E_\alpha)$ for both ^{6}He and ^{6}Li. The difference is understandable because the reanalyzed lower energy data [18] were not available to Woo *et al.*. The interpolated line for ^{6}He lies somewhat above the upper limit from [16] at 198 MeV, but in general the data form a consistent set. The cross section for ^{6}Li at 620 MeV lies significantly above the fitted exponential.

Total cross sections for ^{7}Li and ^{7}Be are found by extrapolating the differential cross sections to zero degrees, integrating from $0-90°$ in the c.m. frame, and doubling, as in the $A = 6$ analysis. Results are shown in Fig. 7 and in Table II along with other measurements from 60 to 600 MeV. Our result at 159.3 MeV is in excellent agreement with those of Glagola [14] near 160 MeV; an exponential describes the entire data set very well. Our experiment yields a significantly tighter upper bound for the ^{7}Be cross section near 600 MeV than that given in [19], and a new limit for ^{7}Li. As expected, since the channels are isospin mirrors, the ^{7}Li and ^{7}Be cross sections are similar in size and energy dependence. Weighted exponential fits yield:

$$\sigma_{^7\mathrm{Li}} = 299\exp(-0.0362E_\alpha)\ \mathrm{mb}, \tag{5}$$

$$\sigma_{^7\mathrm{Be}} = 208\exp(-0.0343E_\alpha)\ \mathrm{mb}. \tag{6}$$

These results are quite similar to that reported in Ref. [16]: $260\exp(-0.035E_\alpha)$mb.

Since ^{6}He decays to ^{6}Li by β^- emission, with a half-life of about 807 msec, the $^4\mathrm{He}(\alpha, pp)^6\mathrm{He}$ and $^4\mathrm{He}(\alpha, \{d, pn\})^6\mathrm{Li}$ reactions are both a source of ^{6}Li produced in the cosmic rays. Therefore, the sum of ^{6}Li and ^{6}He cross sections at each energy is also given in Table I. In cases where ^{6}He measurements are not available, the sum includes an estimate for the ^{6}He contribution, equal to 12% of the ^{6}Li cross section (103.0 and 619.7 MeV) or equal to the reported upper limit (0.2 mb) for ^{6}He at 198.4 MeV.

In Fig. 8 we show the mass–6 cross sections, the sum of the cross section for ^{6}Li and ^{6}He. As was already clear from the fits shown in Fig. 6, an exponential fit would lie significantly

(about three standard deviations) below the point at 620 MeV. The fit shown includes an energy independent cross section and describes the data well; it should be useful for applications. It would be desirable to use a form that more accurately reflects possible physical processes at high energy, but the data is sufficient to fix only one parameter beyond the low energy exponential; adding a constant cross section is the simplest choice. The resulting constant cross section is much smaller than the uncertainty in the low energy cross sections.

The sum of the ^{4}He$(\alpha,p)^7$Li and ^{4}He$(\alpha,p)^7$Be cross sections is also given in Table II for each energy. Since ^{7}Be decays by electron capture to ^{7}Li with a half-life of 53.3 days, these are the relevant cross sections for calculation of ^{7}Li production in cosmic rays. Finally, Fig. 8 shows the sum of the ^{7}Li and ^{7}Be cross sections, an exponential fit to the data, and a fit including a constant cross section.

The exponential or exponential-plus-constant cross section forms shown in Fig. 8 provide a convenient description of the data for use in applications. For the total mass-6 and mass-7 yields these are

$$\sigma_{mass-6} = 0.014 + 75\exp\left(-0.0159E_\alpha\right) \text{ mb}, \tag{7}$$

$$\sigma_{mass-7} = 0.005 + 514\exp(-0.0354E_\alpha) \text{ mb}, \tag{8}$$

$$\sigma_{mass-7} = 510\exp(-0.0354E_\alpha) \text{ mb}. \tag{9}$$

IV. SUMMARY AND DISCUSSION

With these new cross sections for production of $A = 6, 7$ by the $\alpha + \alpha$ reaction, it is possible to calculate the amounts of ^{6}Li and ^{7}Li produced in early-galaxy cosmic rays more accurately. The need to extrapolate cross sections to high energies is no longer a significant factor in the uncertainty. Because of the smaller cross sections obtained here for mass-6 the

the production of ^{6}Li will be significantly smaller than would be obtained with cross sections from the the summary of Read and Viola [11].

To illustrate these points, we use a cosmic ray spectrum peaked around 200 MeV/nucleon (specifically, Fig. 2b of Ref. [12], the curve labeled $\Lambda = 10$ g/cm^2. The product of this spectrum and various cross sections was integrated over energy. A comparison of results using our cross sections and those of Read and Viola [11] is useful, because most calculations of cosmic ray nucleosynthesis have used the Read-Viola cross sections. Both an exponential fit (not shown) and the exponential plus background fit (Eq. 7) shown in Fig. 8 yield about 50% of the ^{6}Li obtained using the cross sections of Read and Viola. For ^{7}Li the differences are relatively small, because the reaction cross sections are already quite small by 200 MeV, and because upper limits for ^{7}Be at higher energies had been reported. For the cosmic ray spectrum employed here (and using the Read-Viola cross sections for $E < 70$ MeV) the production rates of ^{7}Li and ^{6}Li are nearly equal, with ^{7}Li production larger by about 10%.

Detailed calculations of the effects of the new cross sections and the suggested renormalizations of lower energy cross sections [18] will be reported at a later date [20]. In general they will result in a significant reduction of the calculated cosmic ray production of ^{6}Li by $\alpha + \alpha$ reactions. The reduction is dependent on the cosmic ray spectrum and will be largest when it has a large component above 200 MeV. The energy dependence of the cross sections at high energies, that is, the expected limit of the observed exponential behavior, remains an issue. We are not aware of detailed studies of this phenomenon. In the case of mass-6, a deviation from exponential behavior is required by the data, and we have assumed a constant value at higher energies. In the case of mass-7, there is no convincing evidence for such a deviation. However, given the deviation seen for mass-6, we have provided for mass-7, as alternatives, pure exponential and constant-plus-exponential fits to the data. For the cosmic ray spectrum we have chosen, the difference between the two assumptions affects the mass-7 yield at only the 0.4% level.

The production of ^{6}Li and ^{7}Li by $\alpha + \alpha$ reactions will play a vital role in reaching an understanding of the synthesis of LiBeB and the nature of the cosmic rays. New data on the

abundances of LiBeB in metal-poor stars formed early in the history of the galaxy (see [7] for a summary) have led to the following scenario for the production of LiBeB. Essentially all of the ^{6}Li, Be, and ^{10}B, and some of the ^{7}Li and ^{11}B observed in these stars is produced by cosmic ray nucleosynthesis. Big Bang nucleosynthesis contributes the remaining ^{7}Li, the amount depending on whether lithium is destroyed during stellar evolution. Neutrino induced spallation in supernovae produces the remainder of the ^{11}B. The production of lithium by cosmic rays places strong constraints on this scenario, with $\alpha + \alpha$ interactions being particularly important in the standard GCR scenario because the abundances of CNO nuclei are relatively low [6]. Since ^{6}Li is more fragile than ^{7}Li, its survival in a star can be used to limit the amount of ^{7}Li depletion. In order to use ^{6}Li in this way, the initial amount of ^{6}Li must be estimated from a model for cosmic ray nucleosynthesis and then compared to its observed abundance. The resulting ^{6}Li depletion can be used to determine ^{7}Li depletion and eventually, the primordial abundance of ^{7}Li. In recent models of both types (see for example [8,10]) the production of ^{6}Li is marginally sufficient or too small, even assuming none has been destroyed during stellar evolution. The downward changes in the predictions that will result from the present measurements may, therefore, have important consequences.

ACKNOWLEDGMENTS

We would like to thank P. Danielewicz, B. D. Fields, R. Ramaty, and V. E. Viola for useful discussions; M. Hellstrom, R. A. Kryger, J. S. Winfield, and the staff of the National Superconducting Cyclotron Laboratory for assistance with various aspects of the data collection; and R. J. Peterson, R. A. Ristinen, and C. J. Gelderloos for useful discussions concerning analysis. This work was supported by grants from the National Science Foundation and the U.S. Department of Energy.

REFERENCES

[1] H. Reeves, W. A. Fowler, and F. Hoyle, Nature **226**, 727(1970).

[2] M. Meneguzzi, J. Audouze, and H. Reeves, Astron. Astrophys. **15**, 337 (1971).

[3] Sam M. Austin, Prog. Part. Nucl. Phys. **7**, 1(1981).

[4] H. Reeves, Rev. Mod. Phys. **66**, 193 (1994).

[5] D. K. Duncan, D. L. Lambert, and M. Lemke, Astrophys. J. **401**, 584 (1992).

[6] G. Steigman, and T. Walker, Astrophys. J. **385**, L13(1992).

[7] R. Ramaty, B. Kozlovsky, and R. Lingenfelter, Phys. Today **51**, April 1998, p. 30.

[8] R. Ramaty, S. T. Scully, R. E. Lingenfelter, and B. Kozlovsky, Astrophys. J. **534**, 747(2000).

[9] Brian D. Fields and Keith A. Olive, Astrophys. J. **516**, 797(1999).

[10] Brian D. Fields and Keith A. Olive, New Astronomy **4**, 255(1999).

[11] S. M. Read and V. E. Viola, Jr., At. Data Nucl. Data Tables **31**, 359 (1984).

[12] Brian D. Fields, Keith A. Olive, and D. N. Schramm, Astrophys. J. **435**, 185 (1994).

[13] C. H. King, Sam M. Austin, H. H. Rossner, and W. S. Chien, Phys. Rev. C **16**, 1712 (1977).

[14] B. G. Glagola, G. J. Mathews, H. F. Breuer, V. E. Viola, Jr., P. G. Roos, A. Nadasen, and Sam M. Austin, Phys. Rev. Lett. **41**, 1698 (1978); B. G. Glagola, V. E. Viola, Jr., H. Breuer, N. S. Chant, A. Nadasen, P .G. Roos, Sam M. Austin, and G. J. Mathews, Phys. Rev. C **25**, 34 (1982).

[15] J. P. Alard, M. M. Avome Nze, J. P. Costilhes, J. Fargeix, and G. Roche, Nucl. Instrum. Methods **160**, 419 (1979).

[16] L. W. Woo, K. Kwiatkowski, S. H. Zhou, and V. E. Viola, Jr., Phys. Rev. C **32**, 706 (1985).

[17] A. Nadasen, P. G. Roos, B. G. Glagola, G. J. Mathews, V. E. Viola, Jr., H. G. Pugh, and P. Frisbee, Phys. Rev. C **18**, 2792 (1978).

[18] D. J. Mercer, Sam M. Austin, and B. G. Glagola, Phys. Rev. C **55**, 946 (1996).

[19] F. Yiou and G. M. Raisbeck, paper O.G. 133, *Proc. 15th Int. Cosmic Ray Conf.*, (Plovdiv, Bulgaria, 1977) .

[20] T. P. Walker (unpublished).

TABLES

TABLE I. Total cross sections (mb) for the ^{4}He$(\alpha, pp)^6$He and ^{4}He$(\alpha, \{d, pn\})^6$Li (g.s.+3.56) reactions as a function of bombarding energy. Their sum is also given for convenience, with estimates made for the ^{6}He contribution as described in the text where data are not available. The errors for the present experiment include an 8% uncertainty in the normalization, added in quadrature.

Energy (MeV)	^{6}He	^{6}Li	^{6}He+^{6}Li
61.5	1.7 ± 0.2[a]	21.5 ± 2.2[b]	23.2 ± 2.2
80.8	2.0 ± 0.6[b]	18.9 ± 1.4[b]	20.9 ± 1.5
103.0	–	12 ± 1[c]	14 ± 2
118.9	1.2 ± 0.3[b]	10.5 ± 0.6[b]	11.7 ± 0.7
139.2	1.1 ± 0.3[b]	8.4 ± 0.5[b]	9.5 ± 0.6
158.2	0.8 ± 0.2[b]	5.2 ± 0.3[b]	6.0 ± 0.4
159.3	$\mathbf{0.79 \pm 0.08}$[d]	$\mathbf{5.3 \pm 0.4}$[d]	$\mathbf{6.1 \pm 0.5}$
198.4	< 0.2[e]	3.4 ± 0.8[e]	3.6 ± 0.8
279.6	$\mathbf{0.11 \pm 0.03}$[d]	$\mathbf{0.64 \pm 0.08}$[d]	$\mathbf{0.75 \pm 0.09}$
619.7	–	$\mathbf{0.015 \pm 0.004}$[d]	$\mathbf{0.018 \pm 0.004}$

[a]Reference [14].

[b]Reference [14] renormalized according to [18].

[c]Reference [15].

[d]Present experiment (boldface).

[e]Reference [16].

TABLE II. Total cross sections (mb) for the $^4He(\alpha,p)^7Li$ (g.s.+0.48) and $^4He(\alpha,n)^7Be$ (g.s.+0.43) reactions as a function of bombarding energy. Their sum is also given. The errors in the present results include an 8% uncertainty in the normalization, added in quadrature. Upper limits from the present work are at the one standard deviation level.

Energy (MeV)	^7Li	^7Be	$^7Li+^7Be$
61.5	33.2 ± 2.7[a]	23.1 ± 2.6[a]	56.3 ± 3.7
80.8	16.8 ± 1.1[a]	15.6 ± 1.7[b]	32.4 ± 2.0
103.0	6 ± 1[c]	6 ± 1[c]	12 ± 1.4
118.9	4.0 ± 0.3[a]	3.6 ± 0.3[b]	7.6 ± 0.4
139.2	2.0 ± 0.2[a]	1.8 ± 0.2[b]	3.8 ± 0.3
158.2	0.95 ± 0.08[a]	0.83 ± 0.07[b]	1.78 ± 0.11
159.3	$\mathbf{1.00 \pm 0.10}$[d]	$\mathbf{0.87 \pm 0.09}$[d]	$\mathbf{1.87 \pm 0.17}$
198.4	0.25 ± 0.06[e]	0.35 ± 0.08[e]	0.60 ± 0.10
279.6	$\mathbf{0.028 \pm 0.014}$[d]	$\mathbf{0.022 \pm 0.009}$[d]	$\mathbf{0.050 \pm 0.017}$
400.0	–	< 0.02[f]	–
600.0	–	< 0.014[f]	–
619.7	$\mathbf{< 0.004}$[d]	$\mathbf{< 0.003}$[d]	$\mathbf{< 0.006}$

[a]Reference [14].

[b]Ref. [14] renormalized according to [18].

[c]Reference [15].

[d]Present experiment (boldface).

[e]Reference [16].

[f]Reference [19].

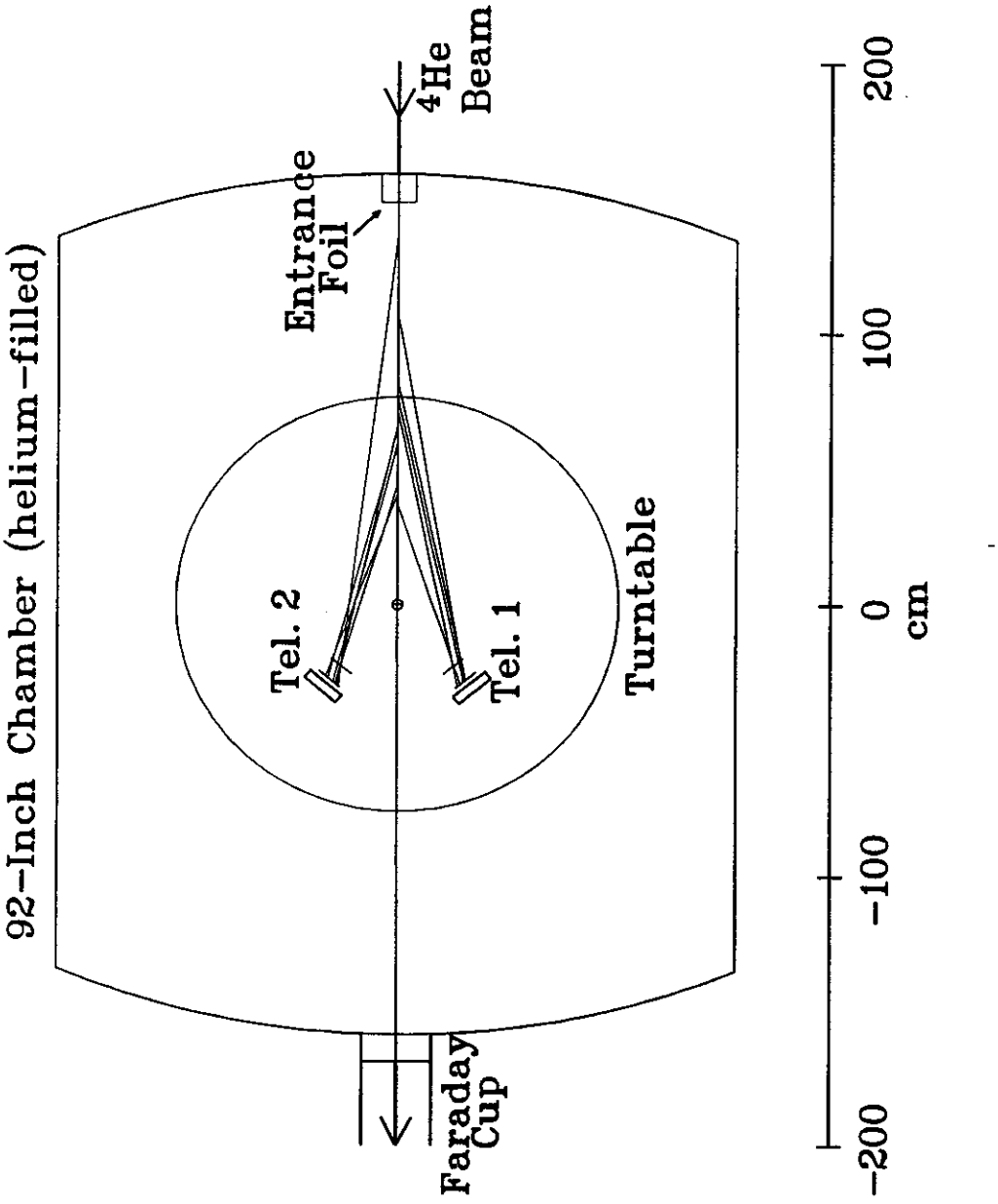

FIG. 1. Schematic of the experimental setup. The scattering chamber had a volume of 13 m^3, and was filled with ^{nat}He gas during normal data collection. Two detector telescopes were mounted on a turntable inside the chamber, viewing an effective target region approximately 150 cm long. Several reconstructed ^{7}Li ejectile tracks are shown.

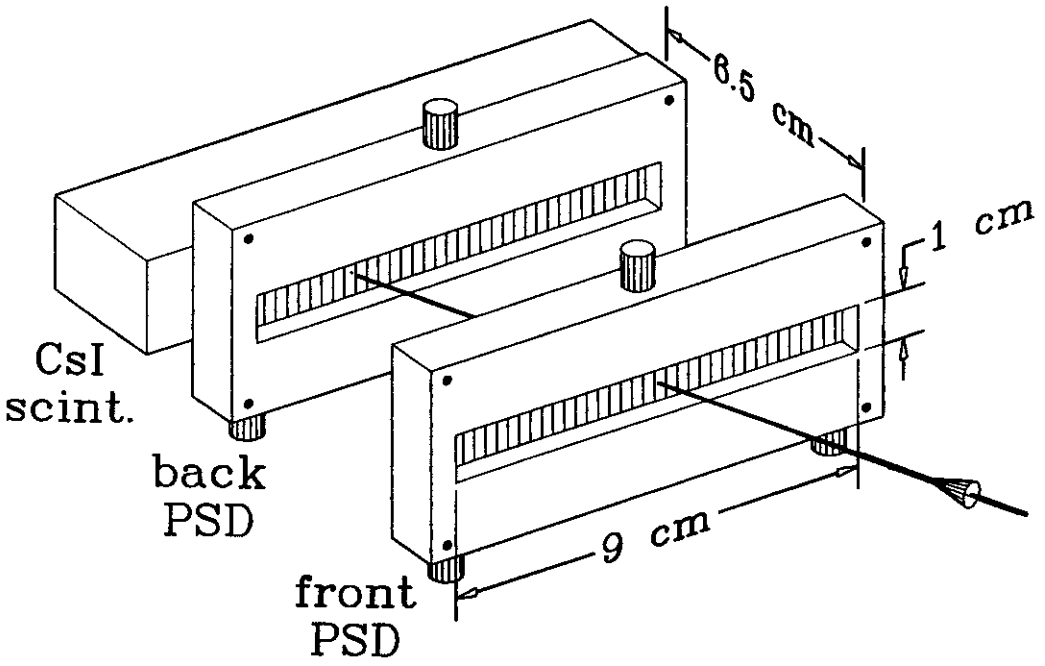

FIG. 2. Detail of a telescope, consisting of two Micron, Inc. Model TT position-sensitive detectors and a CsI(Tl) scintillator crystal; for more details see the text. An example ejectile track is shown.

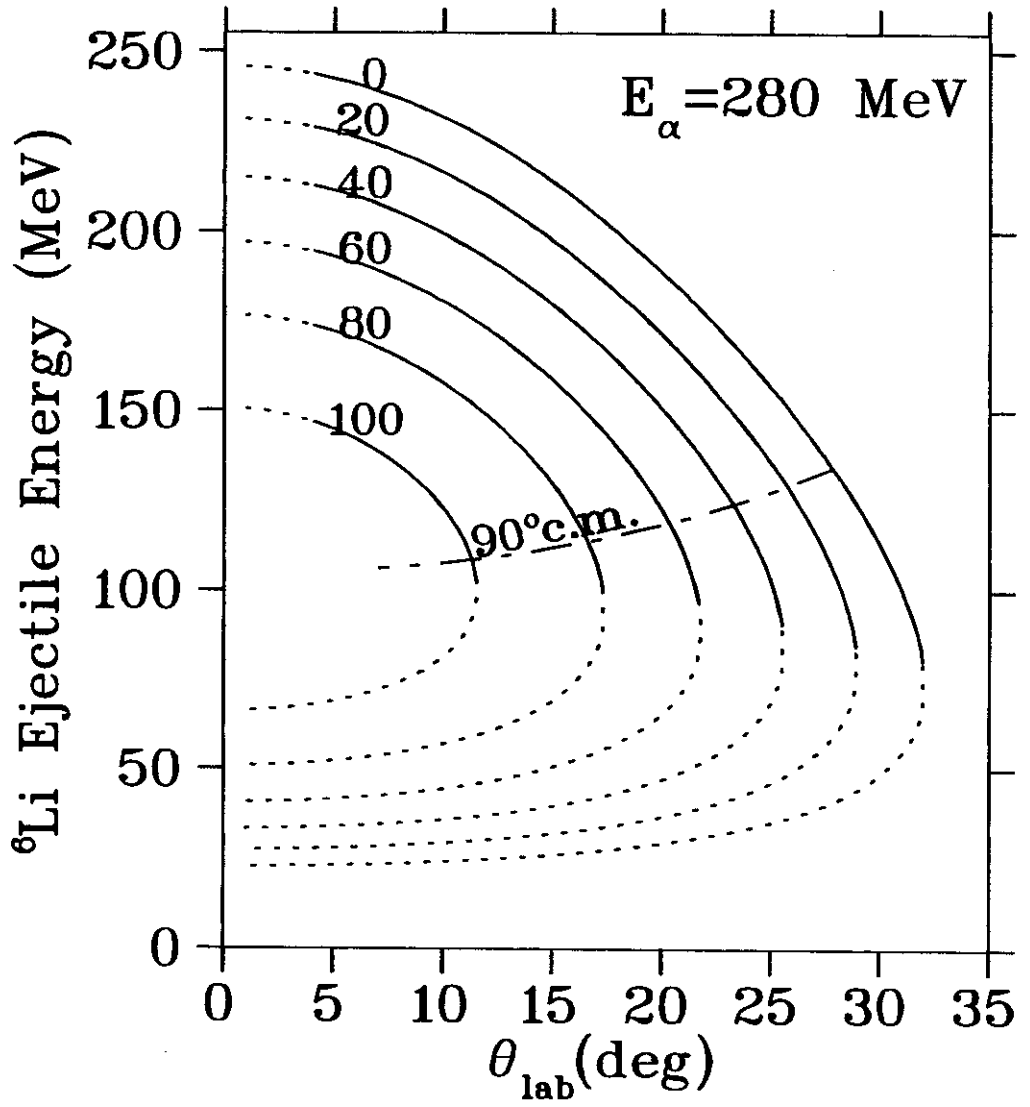

FIG. 3. Kinematics for the ^{4}He$(\alpha, \{d, pn\})^6$Li reaction at a bombarding energy of 280 MeV. The dot-dash curve indicating 90° in the center of momentum frame was determined as described in the text. The two-body ^{6}Li+d exit channel follows the curve labeled "0". The other curves are for the three-body $^6\mathrm{Li} + p + n$ exit channel, approximated by assuming a deuteron with pseudo-excitation energy up to 100 MeV. Solid portions of the curves indicate the region of kinematic acceptance of our detectors. These curves were not used in the analysis and are given for orientation.

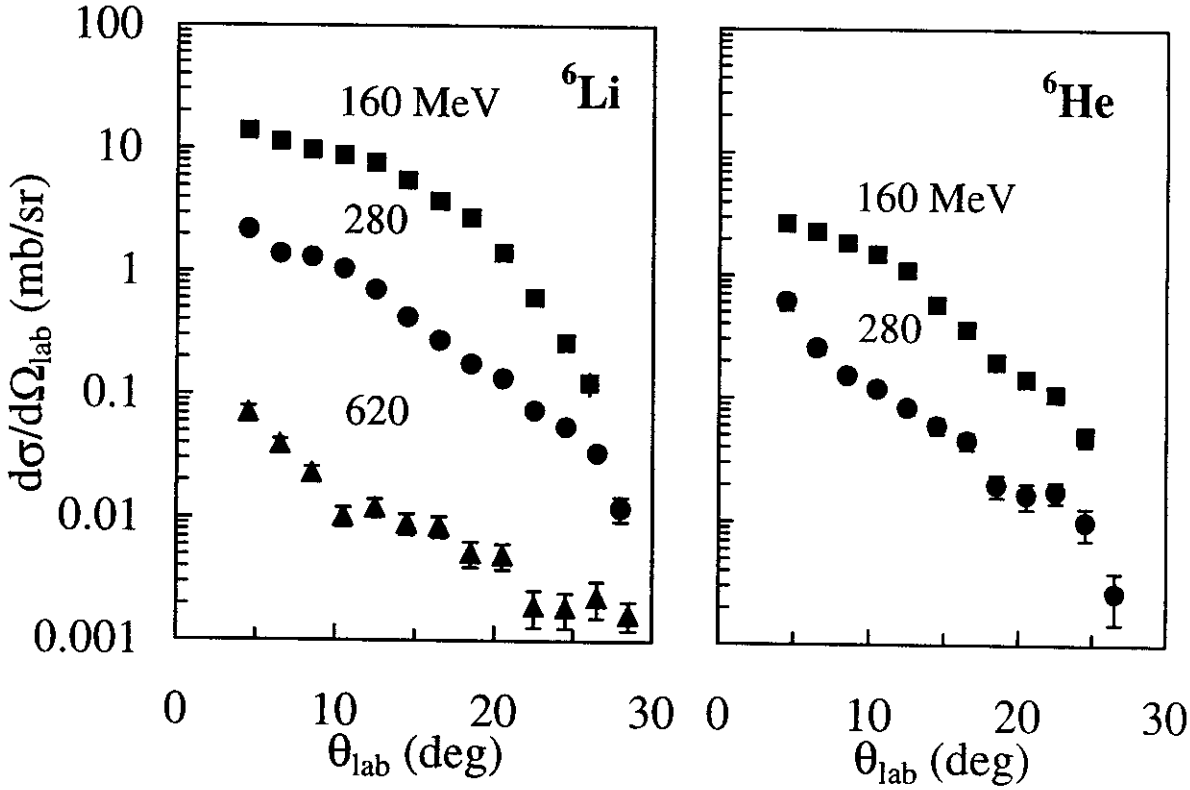

FIG. 4. Laboratory differential cross sections for the $^4\mathrm{He}(\alpha, \{d, pn\})^6\mathrm{Li}$ and $^4\mathrm{He}(\alpha, pp)^6\mathrm{He}$ reactions from the present experiment. Error bars show statistical uncertainty.

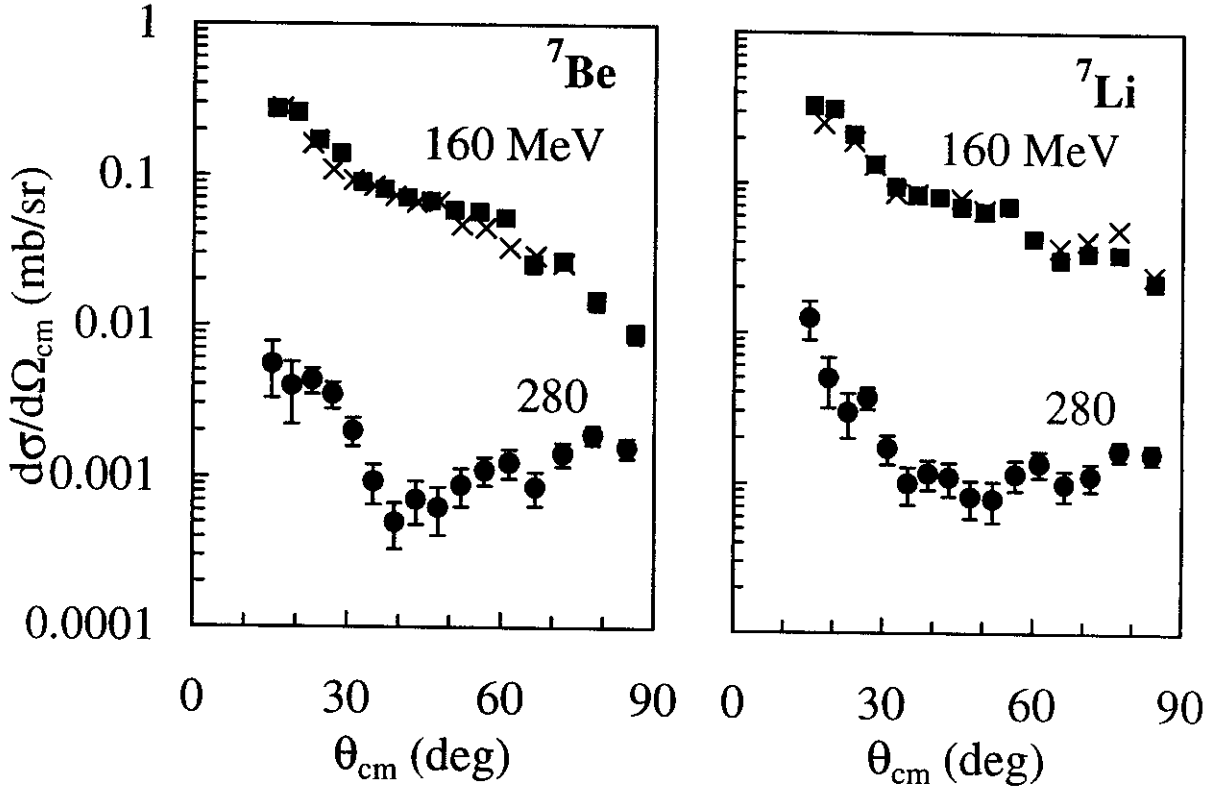

FIG. 5. Differential cross sections for the ^{4}He$(\alpha,n)^7$Be and ^{4}He$(\alpha,n)^7$Li reactions. Squares and circles are from the present experiment, and $\times$'s are from Ref. [14].

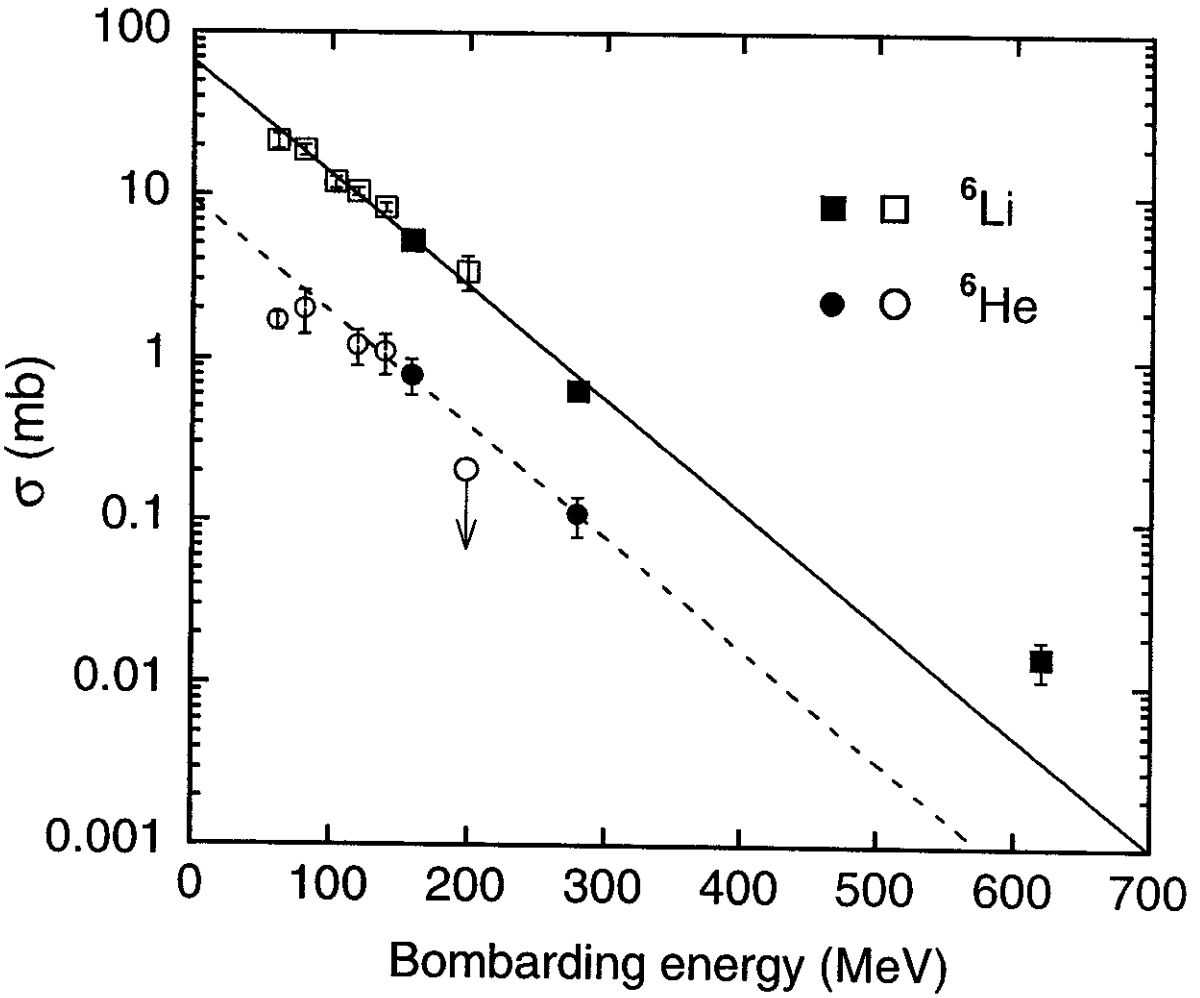

FIG. 6. Total cross sections for ^{4}He$(\alpha, \{d, pn\})^6$Li (squares) and ^{4}He$(\alpha, pp)^6$He (circles). Solid symbols are from the present experiment, and the open symbols are from previous work as summarized in Table I. The lines are exponential fits as described in the text (Eqs. 3, 4).

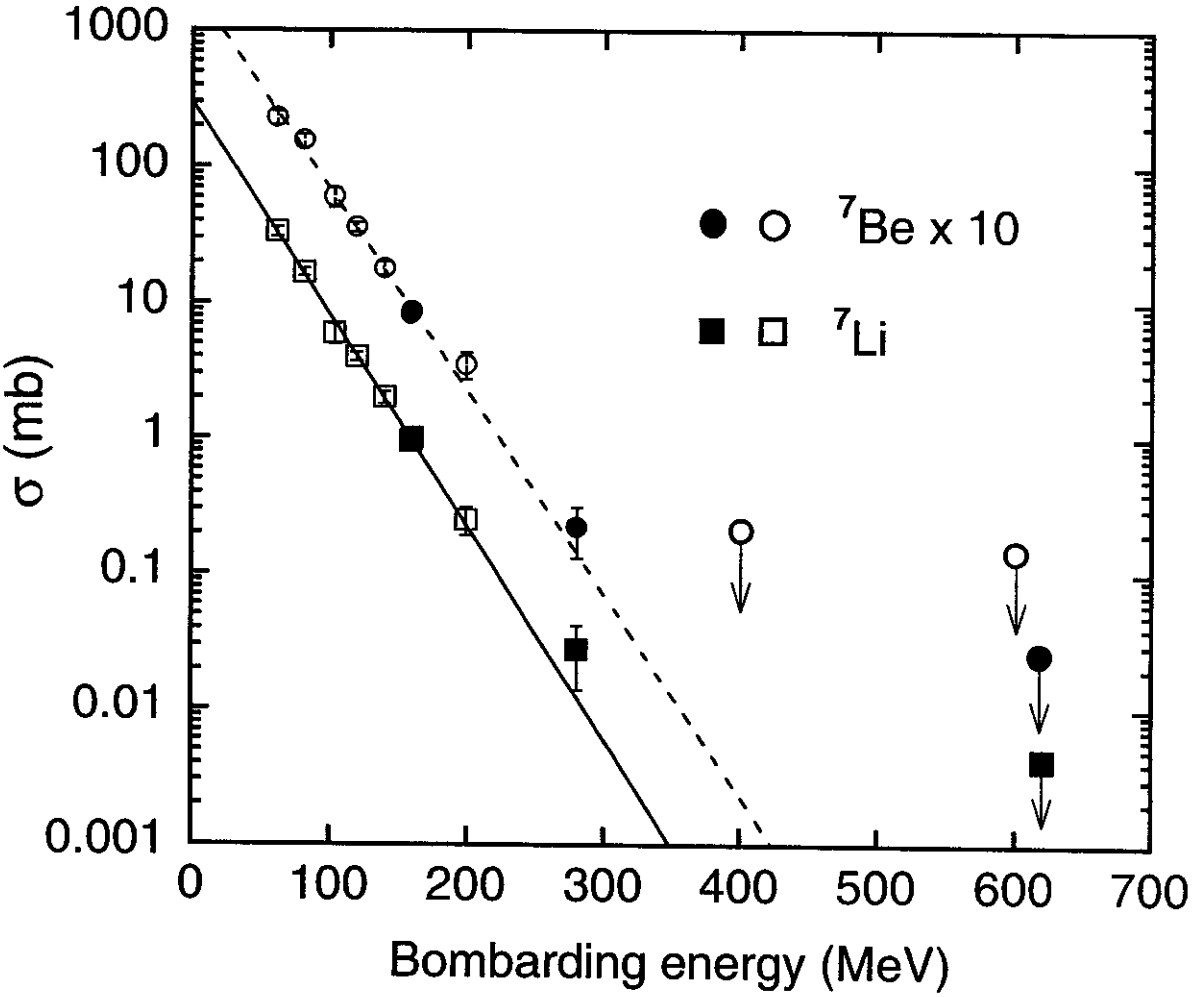

FIG. 7. Total cross sections for ^{4}He$(\alpha,n)^7$Be (circles) and ^{4}He$(\alpha,n)^7$Li (squares). All ^{7}Be values are multiplied by 10 for clarity. Solid symbols are from the present experiment, and the open symbols are from previous work as summarized in Table II. The lines are exponential fits as described in the text (Eqs. 5, 6).

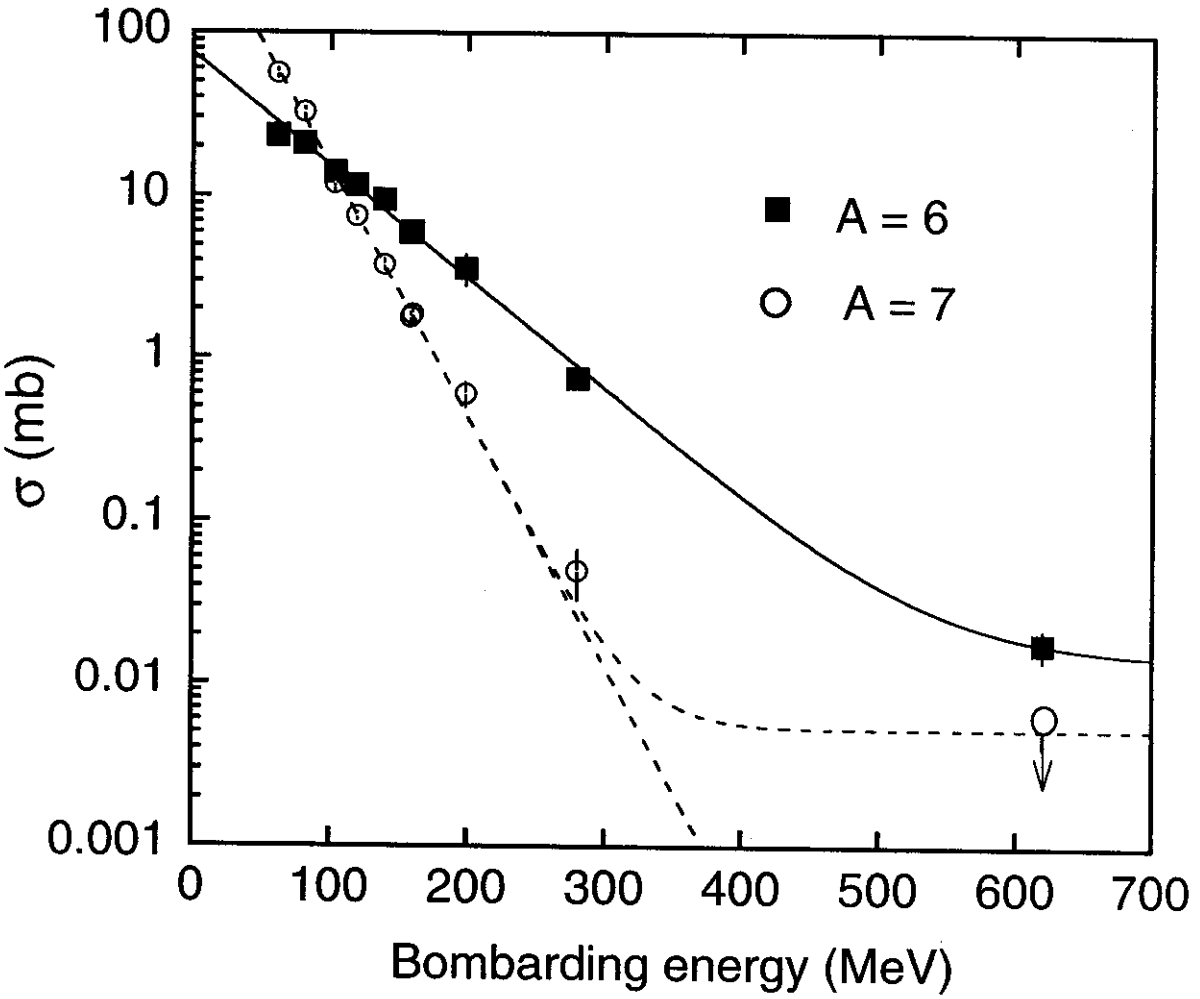

FIG. 8. Total cross sections for mass-6 and mass-7. The fits are described in the text (Eqs. 7-9).